K. J. Willis ; N. Sule ; S. C. Hagness ; I. Knezevic;
Coupled simulation of carrier transport and electrodynamics: the EMC/FDTD/MD technique.
Proc. SPIE 9357, Physics and Simulation of Optoelectronic Devices XXIII, 935706 (March 16, 2015); doi:10.1117/12.2083396.

# Coupled simulation of carrier transport and electrodynamics: the EMC/FDTD/MD technique

K. J. Willis,* N. Sule,†, S. C. Hagness, and I. Knezevic‡

Department of Electrical and Computer Engineering, University of Wisconsin– Madison, Madison, Wisconsin 53706, USA

## ABSTRACT

In order to understand the response of conductive materials to high-frequency electrical or optical excitations, the interplay between carrier transport and electrodynamics must be captured. We present our recent work on developing EMC/FDTD/MD, a self-consistent coupled simulation of semiclassical carrier transport, described by ensemble Monte Carlo (EMC), with full-wave electrodynamics, described by the finite-difference time-domain (FDTD) technique and molecular dynamics (MD) for sub-grid-cell interactions. Examples of room-temperature terahertz-frequency transport simulation of doped silicon and back-gated graphene are shown.

**Keywords:** terahertz, multiphysics, transport, FDTD

## 1. INTRODUCTION

Conductive materials (semiconductors, semimetals, and metals) and their nanostructures are used for a variety of electronic, optoelectronic, and plasmonic applications. In these systems, carriers of charge (electrons and holes) interact with applied electromagnetic fields, lattice vibrations, other charge carries and charged impurities, and various structural defects. In order to understand the response of conductive materials to high-frequency electrical or optical excitations, where the fields might vary considerably over the scale of the carrier relaxation time, one must fully account for the interplay between carrier transport and electrodynamics.

In this paper, we present our recent work on developing a self-consistent coupled simulation of semiclassical carrier transport with full-wave electrodynamics.[1–7] Transport is described by the ensemble Monte Carlo (EMC) technique, a stochastic solution to the Boltzmann transport equation. During the simulation, an ensemble of carriers exhibit periods of free flight under the influence of the local electromagnetic fields, interrupted by scattering events. Full-wave electrodynamics is described by the finite-difference time-domain (FDTD) technique, a well-known grid-based explicit numerical approach to solving Maxwell's curl equations. In realistic materials, two charge carriers or carriers and ions can be found at distances smaller than the grid-cell size; in order to capture these short-range interactions, the molecular dynamics (MD) technique is employed. We discuss the requirements for a successful coupling of the constituent techniques into a self-consistent EMC/FDTD/MD solver, and show examples of *ac* transport in doped silicon and graphene.

## 2. CONSTITUENT TECHNIQUES OF EMC/FDTD/MD

### 2.1 Ensemble Monte Carlo (EMC)

EMC is a powerful stochastic method used for numerical simulation of carrier transport in semiconductors in the scattering-limited (diffusive) regime.[8–15] It has been used for almost four decades to accurately simulate carrier transport properties of bulk semiconductors and semiconductor-based devices, and it provides a benchmark for drift-diffusion and hydrodynamics equations approaches.[9] EMC yields the numerical solution to the Boltzmann transport equation

$$\frac{\partial f}{\partial t} + \vec{v} \cdot \nabla_{\vec{r}} f + \vec{F} \cdot \nabla_{\vec{p}} f = \left.\frac{\partial f}{\partial t}\right|_{\text{scatter}} \tag{1}$$

* Current affiliation: AWR Corporation, Mequon, Wisconsin 53092, USA; † Current affiliation: James Franck Institute, University of Chicago, Chicago, Illinois 60637, USA; ‡ Corresponding author: knezevic@engr.wisc.edu

where $f(\vec{r},\vec{p},t)$ is the semiclassical distribution function, $\vec{v}$ is the carrier velocity, and $\vec{F}$ is the total force acting on the carrier. $f(\vec{r},\vec{p},t)$ describes the probability that a carrier exists within $d^3\vec{r}$ of position $\vec{r}$ and within $d^3\vec{p}$ of momentum $\vec{p}$ at time $t$. $f(\vec{r},\vec{p},t)$ evolves in time according to Eq. (1) as a result of diffusion (included in the second term) and carrier drift due to external forces (described by the third term). The collision integral (described by the term on the right hand side of the equation) describes the impact of the material-specific scattering mechanisms on the carrier ensemble.

EMC simulates carrier dynamics in semiconductors by tracking the evolution of a large ensemble of particles [typically $O(10^5)$] through time. Each carrier undergoes a series of scattering events and free flights. A random number generator is used to calculate the duration of each free flight, choose the mechanism for the next scattering event, and update the particle's momentum and energy as needed, according to the appropriate statistical probabilities. Momentum is updated during free flight according to the Lorentz force,

$$\vec{F} = q(\vec{E} + \vec{v} \times \vec{B}), \tag{2}$$

where $q$ is the carrier charge, while $\vec{E}$ and $\vec{B}$ are the electric and magnetic fields, respectively. Macroscopic quantities of interest (such as charge density and drift velocity) are readily extracted via ensemble averages.

### 2.2 The finite-difference time-domain technique (FDTD)

FDTD is a highly accurate and efficient computational technique for modeling electromagnetic wave interactions with physical structures. Advances in absorbing boundary conditions, dispersive and nonlinear materials modeling, low-numerical-dispersion schemes, unconditionally stable schemes, and incident wave source conditions make FDTD a highly attractive tool for electromagnetic analysis.[16] FDTD is a direct numerical solution of the time-dependent Maxwell's curl equations,

$$\mu\frac{\partial\vec{H}}{\partial t} = -\nabla\times\vec{E} - \vec{M}, \quad \epsilon\frac{\partial\vec{E}}{\partial t} = \nabla\times\vec{H} - (\vec{J} + \sigma\vec{E}), \tag{3}$$

where $\vec{E}$ and $\vec{H}$ are the electric and magnetic fields, respectively, $\epsilon$, $\mu$, and $\sigma$ are the permittivity, permeability, and conductivity of the medium, and $\vec{J}$ and $\vec{M}$ are the electric and magnetic source current densities.

The fully explicit FDTD algorithm is obtained by numerically approximating the spatial partial derivatives in Eqs. (3) with centered finite differences, and numerically integrating the resulting system of spatial difference equations with respect to time via a centered finite-difference approximation of the temporal partial derivatives. The staggering of $\vec{E}$ and $\vec{H}$ in time yields an efficient leapfrog time-marching scheme wherein all of the $\vec{E}$ components are updated at time step $n$ (corresponding to a physical time of $n\Delta t$) using previously stored $\vec{H}$ data, and then all of the $\vec{H}$ components are updated at time step $n + 1/2$ using the just computed $\vec{E}$ data.

The grid-based vector quantities – $\vec{E}$, $\vec{H}$, $\vec{J}$, and $\vec{M}$ – are positioned relative to each other according to the Yee grid cell shown in Fig. 1.[17] Figure 1 illustrates the staggered sampling of $\vec{E}$ and $\vec{H}$ over one grid cell in a 3D Cartesian spatial lattice. Each vector component of $\vec{J}$ is spatially collocated with the corresponding component of $\vec{E}$; $\vec{M}$ and $\vec{H}$ are similarly collocated. Position within the discrete grid is defined in terms of grid indices $(i,j,k)$. The grid point at $(i,j,k)$ has physical location $[x(i),y(j),z(k)]$ where $x(i) = i\Delta x$, $y(j) = j\Delta y$, and $z(k) = k\Delta z$. The 3D FDTD grid used in this EMC/FDTD/MD implementation is defined with cubic grid cells, where $\Delta x = \Delta y = \Delta z$.

Domain boundaries may be treated by any of several techniques, the most popular of which is the perfectly matched layer (PML) absorbing boundary condition.[18] There are many variations on the original PML formulation, designed to attenuate outward-propagating radiation and minimize reflections from the domain boundary under various special circumstances.[19] Thus the main grid is electromagnetically isolated from the grid boundary, permitting finite-grid representation of an infinite space. Other boundary conditions, such as fully reflecting boundaries or transparent periodic boundaries, may alternatively be enforced, to suit a particular application.[16]

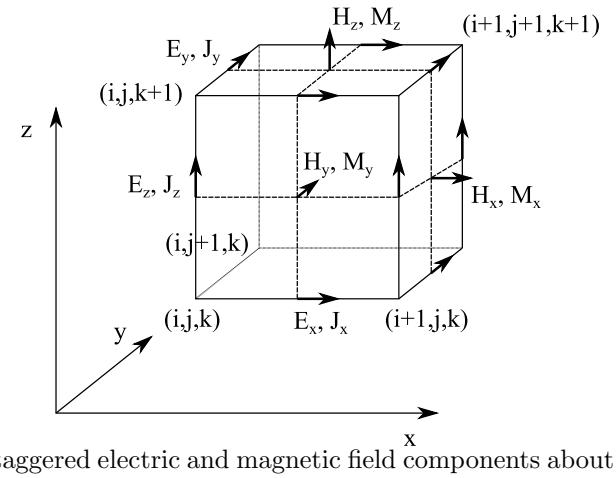


Figure 1: Illustration of the staggered electric and magnetic field components about a single Yee cell in a 3D space lattice. The axis origin is positioned at index $(i, j, k)$, and the opposite corner has index $(i+1, j+1, k+1)$. Each electric field component, on the edge of the cell, is surrounded by four circulating magnetic field components. Likewise, each magnetic field component, normal to the face of the cell, is surrounded by four circulating electric field components. Reprinted with permission from [4], K. J. Willis, S. C. Hagness, and I. Knezevic, "Multiphysics simulation of high-frequency carrier dynamics in conductive materials," J. Appl. Phys. 110, 063714 (2011). ©2011, American Institute of Physics.

### 2.3 Molecular dynamics (MD)

In metals and semiconductors with higher doping densities, the strong Coulomb force between charged particles significantly impact materials properties.[20] The difficulty of accurately incorporating the strong Coulomb interaction into computational techniques is a long-standing problem.[20] The molecular dynamics (MD) technique has been described as the ideal and natural way to account for charged particle interactions in materials, and, when combined with EMC, it has predicted materials properties with very high accuracy.[21–23] However, the technique is very computationally intensive, and for that reason it has generally been avoided in the computational electronics community. Additionally, the fully-classical MD implementation cannot accurately describe high-$n_0$ materials, where the exchange interaction between indistinguishable electrons significantly affects bulk properties.[24–26]

Molecular dynamics describes the behavior of collections of particles with binary particle-particle interactions.[27] For an ensemble of electrons and ions, MD finds the pairwise electrostatic force between each carrier and all other carriers and stationary ions in the vicinity. In an ensemble of $N_{\text{elec}}$ electrons and $N_{\text{ion}}$ ions, the MD prediction for the net Coulomb force acting on the $i^{th}$ electron is

$$\vec{F}_i = \sum_{j \neq i}^{N_{\text{elec}}} \frac{q^2}{4\pi\epsilon(\vec{r}_i - \vec{r}_j)^2}\hat{r}_{ij} + \sum_{j=1}^{N_{\text{ion}}} \frac{qQ}{4\pi\epsilon(\vec{r}_i - \vec{r}_j)^2}\hat{r}_{ij} \tag{4}$$

where $Q$ is the ion charge, $\epsilon$ is the static material permittivity, $\hat{r}_{ij} = (\vec{r}_i - \vec{r}_j)/|\vec{r}_i - \vec{r}_j|$, and $\vec{r}_i$ is the position of the $i^{th}$ particle. In the particle solver, the MD forces describe the full electrostatic system. The MD technique avoids assumptions about screening lengths or the number of particles likely to participate in any particular interaction, and it naturally incorporates all collective ensemble behavior.[21,23] In addition, the MD technique has been extended to describe exchange interaction between indistinguishable electrons.[24–26] Even with small numbers of particles, the combined EMC/MD solver has been previously used to accurately predict low-frequency behavior in semiconductors and devices.[21–23]

The fundamental MD calculation is conceptually simple but computationally intensive for large carrier ensembles, scaling with the number of particles as $N^2$.[11,28] It is very time consuming to calculate the force on each particle by iterating through the rest of the ensemble. However, the Coulomb interaction can be divided into a short-range component, which describes interactions among the particles separated by a couple of grid cells,

and a long-range component.[20,22,29] The long-range part of the Coulomb interaction is quickly and accurately described by the field solver, and the short-range part is described by MD. The EMC/FDTD/MD simulation presented here calculates the long-range Coulomb interaction with FDTD and the short-range interaction with MD.[4]

### 2.4 Coupling the techniques

In EMC/FDTD/MD, the three solvers are coupled at every time step to describe carrier dynamics under applied electromagnetic stimulation with full Coulomb interaction among particles (Fig. 2). FDTD electromagnetic fields and MD electrostatic fields accelerate EMC carriers through the Lorentz force, $\vec{F}$, in Eq. (1). EMC carrier motion defines $\vec{J}$, thereby acting to source FDTD fields in Eq. (3), and instantaneous carrier position defines MD fields in Eq. (4). We note that there are three additional elements, critical for self-consistent coupling of the

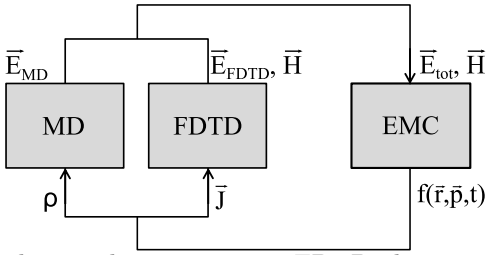


Figure 2: Conceptual flowchart of the simulation process. FDTD electromagnetic fields and MD electrostatic fields combine to accelerate EMC carriers through the Lorentz force. EMC carrier motion sources FDTD fields via $\vec{J}$. Instantaneous carrier positions define MD fields. Reprinted with permission from [4] K. J. Willis, S. C. Hagness, and I. Knezevic, "Multiphysics simulation of high-frequency carrier dynamics in conductive materials," J. Appl. Phys. 110, 063714 (2011). ©2011, American Institute of Physics.

constituent technques: (1) satisfying Gausss law in FDTD through proper field initialization and enforcement of the continuity equation, (2) avoiding double-counting of Coulomb fields in FDTD and MD, and (3) attributing finite radii to electrons and ions in MD for accurate calculation of the short-range Coulomb forces. Morover, there are a number of implementation details of great importance for ensuring numerical efficiency and stability, such as the choice of the right mesh cell size and time step in the simulation. For details, we refer the reader to the comprehensive Ref. 4.

## 3. EXAMPLE: THZ-FREQUENCY CONDUCTIVITY OF DOPED SILICON

We use the 3D EMC/FDTD/MD solver to examine carrier dynamics in doped silicon ($\epsilon_r = 11.7$) under applied electromagnetic fields. The EMC/FDTD/MD region is embedded within the larger FDTD domain. In this work, the EMC describes carrier dynamics in $n-$type silicon at room temperature in the low-field regime. We use the effective mass approximation with first-order nonparabolicity.[8] Acoustic intravalley and zeroth-order intervalley phonon scattering are included via semiclassical scattering rates.[30] All material parameters and constants are taken from Ref. 31. Coulomb interaction is treated via FDTD and MD, and therefore we do not use explicit scattering rates to describe ionized impurity, plasmon, or carrier-carrier scattering. The Pauli exclusion principle is enforced for each scattering event with the rejection technique.[8]

The incident TEM field is linearly polarized; the dominant force applied to the carriers is directed along the direction of polarization ($z$). We drive carrier motion in the coupled region via fields sourced from the total-field scattered-field (TFSF) boundary,[16] which extends the height of the FDTD grid in the direction of polarization. In the open-region simulations discussed here, grid boundaries perpendicular the directions normal to the polarization ($x$ and $y$) are treated with convolutional PML (CPML).[16,19] In order to better represent a bulk material, EMC enforces specular reflection of carriers from the boundaries normal to $x$ and $y$. The boundaries normal to $z$ are treated with periodic boundary conditions in all three solvers, permitting unrestricted carrier motion and continuous electromagnetic interaction in the $z$ direction.

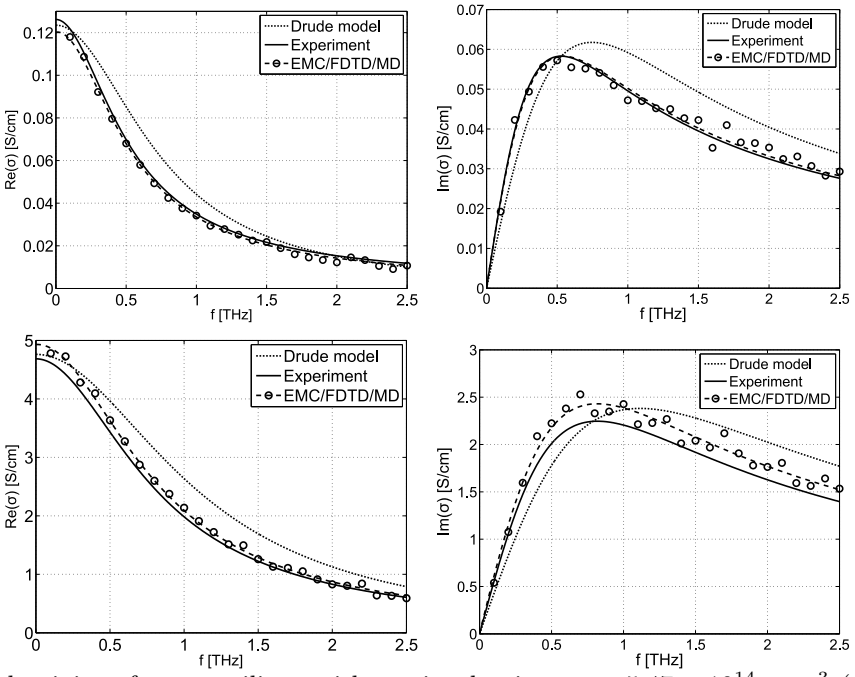


Figure 3: THz conductivity of n-type silicon with carrier density $n_0 = 5.47 \times 10^{14}$ cm$^{-3}$ (top row) and $n_0 = 3.15 \times 10^{16}$ cm$^{-3}$ (bottom row). The dotted lines show the Drude model prediction for the conductivity, based on the known doping density and mobility of the material. The solid lines indicates the analytical fit to the experimental data. $\hat{\sigma}$ calculated by EMC/FDTD/MD is shown with open circles, with a dashed line to guide the eye. The numerical data for $(\hat{\sigma})$ demonstrates excellent agreement with the experimental conductivity. Reprinted with permission from [4], K. J. Willis, S. C. Hagness, and I. Knezevic, "Multiphysics simulation of high-frequency carrier dynamics in conductive materials," J. Appl. Phys. 110, 063714 (2011). ©2011, American Institute of Physics.

We compare the effective conductivity calculated by EMC/FDTD/MD with published experimental results for doped silicon at THz frequencies, obtained via reflecting THz time-domain spectroscopy (THz-TDS).[32] The complex conductivity is given for two $n-$type silicon samples with *dc* resistivities of 8.15 Ω cm and 0.21 Ω cm, corresponding to $n_0 = 5.47 \times 10^{14}$ cm$^{-3}$ (top row in Fig. 3 ) and $n_0 = 3.15 \times 10^{16}$ cm$^{-3}$ (bottom row in Fig. 3). [33] The analytical best fit of the Cole-Davidson model to experimental data is given by Ref. 32. The Cole-Davidson fit can be regarded as a faithful representation of the experimental data, especially at the lower doping density where the experimental data show low noise. EMC/FDTD/MD results are indicated with open circles and a dashed line to guide the eye. The numerical prediction for conductivity shows excellent agreement with experiment.

## 4. EXAMPLE: THZ-FREQUENCY CONDUCTIVITY OF BACK-GATED GRAPHENE

In recent years, considerable attention has been given to the optoelectronic,[34] plasmonic,[35–37] terahertz,[38,39] and radio-frequency[40] applications of graphene. An important factor in evaluating the potential of graphene for these applications, especially in the THz range , is its complex conductivity $\sigma(\omega)$, where $\omega$ is the angular frequency of the excitation.[41,42]

The room-temperature electron dynamics in supported graphene are simulated with charged impurities distributed near the interface between graphene and the substrate. A typical geometry used in experiments consists of exfoliated or chemical vapor deposition (CVD)-grown graphene transferred onto an insulating substrate. The most commonly used insulating substrate is a 300-nm-thick $SiO_2$ layer on top of a Si wafer. In the back of the Si wafer is a gate, used to tune the carrier density in the graphene layer. In the simulations here, the

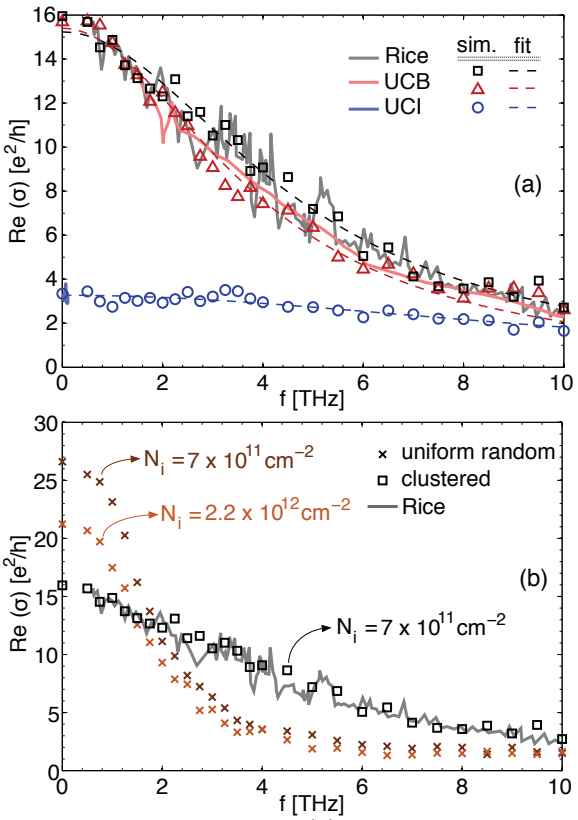


Figure 4: Real part of $\sigma(\omega)$ as a function of frequency. (a) Calculated values based on the EMC/FDTD/MD simulation (squares, triangles, and circles) match, respectively, the experimental data from Refs. [48] (blue: UC Irvine), [49] (red: UC Berkeley), and [50] (black: Rice University). Dashed lines are Drude-model fits to the simulation data. (b) Calculated values with different types of impurity distributions, i.e., clustered (squares, $N_I = 7\times10^{11}\,\mathrm{cm}^{-2}$) and uniform random (x symbols, $N_I = 7\times10^{11}\,\mathrm{cm}^{-2}$ and $N_I = 2.2\times10^{12}\,\mathrm{cm}^{-2}$), compared to the experimental data from the Rice group.[50] Reprinted with permission from [7], N. Sule, K. J. Willis, S. C. Hagness, and I. Knezevic, "Terarahertz-frequency electronic transport in graphene," Phys. Rev. B 90, 045431 (2014). ©2014, American Physical Society.

carrier density is assumed to be tuned by shifting the Fermi level in graphene and the Si-wafer is not explicitly included. Different insulating substrates are modeled by using their appropriate values of the dielectric constants, $\epsilon_s$. Moreover, we take into account the modifications to the Fermi velocity, $v_F$, and dielectric constant of graphene, $\epsilon_g$, due to the substrate.[43,44] The electronic tight-binding Bloch wave functions are used to calculate the electron-intrinsic-phonon scattering rates in graphene based on Fermi's golden rule.[45] For graphene on a substrate, we also calculate the electron-surface optical (SO) phonon scattering rates.[46,47]

Charged impurities in the substrate are modeled by assuming a distribution of singly charged positive ions down to a depth of 10 nm from the graphene layer; impurities deeper than 10 nm have been shown to have a negligible effect on transport.[6] The clustered impurity distributions are generated to have a given average cluster size and a generally Gaussian autocorrelation function.[6]

Figure 4a shows that the real part of $\sigma(\omega)$ calculated by the EMC/FDTD/MD method reproduces experimental data with very good agreement. The impurity density $N_I$ is the only variable parameter and a clustered impurity distribution is assumed.[6] The solid lines are experimental results for graphene on $SiO_2$ at room temperature [blue: UC Irvine (UCI) team;[48] red: UC Berkeley (UCB) team;[49] black: Rice University team[50]]. The symbols (squares, triangles, and circles) represent our simulation results and the dashed lines are fits to the simulation data using the Drude model. We have assumed the same carrier densities as estimated in the experiments, which are $n = 1.8\times10^{12}\,\mathrm{cm}^{-2}$ (UCI),[48] $7.9\times10^{12}\,\mathrm{cm}^{-2}$ (UCB),[49] and $7.7\times10^{11}\,\mathrm{cm}^{-2}$ (Rice).[50]

The impurity densities that yield the best match to the experimental data of UCI, UCB, and Rice are, respectively, $N_I = 5 \times 10^{11}\,\mathrm{cm}^{-2}$, $8 \times 10^{11}\,\mathrm{cm}^{-2}$, and $7 \times 10^{11}\,\mathrm{cm}^{-2}$. These impurity densities, providing an excellent agreement between the simulation and experimental data, are reasonable and quite likely in typical samples.[51]

In 4b, the real part of $\sigma(\omega)$ is compared for clustered (squares) and uniform random (x symbols) impurity distributions with the experimental data from Rice University[50] (solid line). It is clear that, with a uniform random distribution of impurities, a good fit to experiment cannot be obtained even with extremely high values of $N_I$, which presents further evidence that typical supported graphene samples contain clustered impurities.[6] For a given impurity density ($N_I = 7 \times 10^{11}\,\mathrm{cm}^{-2}$), a uniform random impurity distribution results in higher conductivity at low frequencies (f<2 THz) and lower conductivity at high frequencies than the clustered distribution. Based on fitting the calculated frequency-dependent conductivity to the Drude model for the uniform random and clustered impurity distributions for the same $N_I = 7 \times 10^{11}\,\mathrm{cm}^{-2}$, we find that the effective scattering rate for the uniform random distribution ($\Gamma = 2$ THz) is much lower than that for the clustered distribution ($\Gamma = 5$ THz). The higher effective scattering rate for electrons with a clustered impurity distribution is expected, since the electrons trapped near the charged clusters scatter more frequently from the Coulomb potential.

## 5. CONCLUSION

We overviewed our team's recent work on developing a robust and versatile multiphysics simulation technique for a self-consistent description of charge transport coupled to electromagnetic fields. This type of simulation is critical in order to understand the full capabilities of both established and novel conductive materials, such as graphene and layered van der Waals heterostructures,[52] for high-frequency electronic, optoelectronic, and plasmonic applications.

## ACKNOWLEDGMENTS

Early parts of this work were funded by the AFOSR Award No. FA9550-08-1-0052 [3D coupled simulation of THz conductivity of Si (K.J.W., S.C.H., I.K.)] and AFOSR Award No. FA9550-11-1-0299 [2D simulation development and the work on clustered impurities in graphene (N.S., S.C.H., I.K.)]. More recent efforts, including the final stages of the work on the THz conductivity of graphene (N.S., I.K.) and the writing of this manuscript (I.K.), were supported by the U.S. Department of Energy, Office of Basic Energy Sciences, Division of Materials Sciences and Engineering under DOE Award No. DE-SC0008712.

## REFERENCES

1. K. J. Willis, J. Ayubi-Moak, S. C. Hagness, and I. Knezevic, "Global modeling of carrier-field dynamics in semiconductors using EMC-FDTD," *J. Comput. Electron.* **8**, 153–171 (2009).
2. K. J. Willis, S. C. Hagness, and I. Knezevic, "A generalized drude model for doped silicon at terahertz frequencies derived from microscopic transport simulation," *Appl. Phys. Lett.* **102**, 122113 (2013).
3. K. J. Willis, S. C. Hagness, and I. Knezevic, "Terahertz conductivity of doped silicon calculated using the ensemble Monte Carlo/finite-difference time-domain simulation technique," *Appl. Phys. Lett.*, 062106 (2010).
4. K. J. Willis, S. C. Hagness, and I. Knezevic, "Multiphysics simulation of high-frequency carrier dynamics in conductive materials," *J. Appl. Phys.* **110**, 063714 (2011).
5. N. Sule, K. Willis, S. Hagness, and I. Knezevic, "EMC/FDTD/MD simulation of carrier transport and electrodynamics in two-dimensional electron systems," *Journal of Computational Electronics* **12**, 563–571 (2013).
6. N. Sule, S. C. Hagness, and I. Knezevic, "Clustered impurities and carrier transport in supported graphene," *Phys. Rev. B* **89**, 165402 (2014).
7. N. Sule, K. J. Willis, S. C. Hagness, and I. Knezevic, "Terahertz-frequency electronic transport in graphene," *Phys. Rev. B* **90**, 045431 (2014).
8. C. Jacoboni and L. Reggiani, "The Monte Carlo method for the solution of charge transport in semiconductors with applications to covalent materials," *Rev. Mod. Phys.* **55**, 645–705 (1983).
9. M. Lundstrom, *Fundamentals of Carrier Transport*, Cambridge University Press, 2nd ed., 2000.

10. C. Jacoboni and Lugli, *The Monte Carlo Method for Semiconductor Device Simulation*, Springer-Verlag, New York, 1989.
11. K. Tomizawa, *Numerical Simulation of Submicron Semiconductor Devices*, Artech House, 1993.
12. C. K. Birdsall and A. B. Langdon, *Plasma Physics via Computer Simulation*, Adam Hilger, 1991.
13. R. W. Hockney and J. W. Eastwood, *Computer Simulation Using Particles*, Adam Hilger, 1988.
14. K. Hess, *Monte Carlo Device Simulation: Full Band and Beyond*, Kluwer Academic Publishers, 1991.
15. M. V. Fischetti and S. Laux, "Monte Carlo analysis of electron transport in small semiconductor devices including bands structures and space-charge effects," *Phys. Rev. B* **38**, 9721 (1988).
16. A. Taflove and S. C. Hagness, *Computational Electrodynamics: The Finite-Difference Time-Domain Method*, Artech House, 3rd ed., 2005.
17. K. S. Yee, "Numerical solution of initial boundary value problems involving Maxwell's equations in isotropic media," *IEEE Trans. Antennas Propag.* **AP-14**, 302–307 (1966).
18. J. P. Berenger, "Perfectly matched layer for the FDTD solution of wave-structure interaction problems," *IEEE Trans. Antennas Propag.* **44**, 110–117 (1996).
19. J. A. Roden and S. D. Gedney, "Convolutional PML (CPML): an efficient FDTD implementation of the CFS-PML for arbitrary media," *Microw. Opt. Technol. Lett* **27**, 334–339 (2000).
20. D. Vasileska, H. R. Khan, and S. S. Ahmed, "Modeling coulomb effects in nanoscale devices," *J. Comput. Theor. Nanosci.* **5**, 1793–1827 (2008).
21. R. P. Joshi and D. K. Ferry, "Effect of multi-ion screening on the electronic transport in doped semiconductors: A molecular-dynamics analysis," *Phys. Rev. B* **43**(12), 9734–9739 (1991).
22. Lugli and D. K. Ferry, "Dynamical screening of hot carriers in semiconductors from a coupled molecular dynamics and ensemble monte carlo simulation," *Physical Review Letters* **56**, 1295–1297 (1986).
23. D. K. Ferry, A. M. Kriman, and M. J. Kann, "Molecular dynamics extensions of monte carlo simulation in semiconductor device modeling," *Comput. Phys. Commun.* **67**, 119–134 (1991).
24. A. M. Kriman, M. J. Kann, D. K. Ferry, and R. Joshi, "Role of the exchange interaction in the short-time relaxation of a high-density electron plasma," *Phys. Rev. Lett.* **65**, 1619–1622 (1990).
25. A. M. Kriman, R. P. Joshi, M. J. Kann, and D. K. Ferry, "Exchange effects in hot plasmas in semiconductors," *Semicond. Sci. Technol.* **7**, B243–B247 (1992).
26. R. P. Joshi, A. M. Kriman, M. J. Kann, and D. K. Ferry, "Quantum molecular dynamics treatment for the electronic relaxation of high-density plasmas in two-dimensional structures," *Appl. Phys. Lett.* **58**, 2369–2371 (1991).
27. D. C. Rapaport, *The art of molecular dynamics simulation*, Cambridge University Press, 2004.
28. B. J. Alder and T. E. Wainwright, "Studies in molecular dynamics. I. general method.," *J. Chem. Phys.* **31**, 459–466 (1959).
29. W. J. Gross, D. Vasileska, and D. K. Ferry, "A novel approach for introducing the electron-electron andelectron-impurity interactions in particle-based simulations," *IEEE Electron Device Letters* **20**, 463–465 (1999).
30. B. K. Ridley, *Quantum Processes in Semiconductors*, Oxford Science Publications, 4th ed., 1999.
31. M. V. Fischetti and S. Laux, "Monte carlo study of electron transport in silicon inversion layers," *Phys. Rev. B* **48**, 2244–2274 (1993).
32. T. I. Jeon and D. Grischkowsky, "Nature of conduction in doped silicon," *Phys. Rev. Lett.* **78**, 1106–1109 (1997).
33. R. Hull, *Properties of Crystalline Silicon*, IET, 1999.
34. F. Bonaccorso, Z. Sun, T. Hasan, and A. Ferrari, "Graphene photonics and optoelectronics," *Nat. Photon.* **4**, 611–622 (2010).
35. M. Jablan, H. Buljan, and M. Soljačić, "Plasmonics in graphene at infrared frequencies," *Phys. Rev. B* **80**, 245435 (2009).
36. F. H. Koppens, D. E. Chang, and F. J. Garcia de Abajo, "Graphene plasmonics: a platform for strong light–matter interactions," *Nano Lett.* **11**, 3370–3377 (2011).
37. H. Yan, T. Low, W. Zhu, Y. Wu, M. Freitag, X. Li, F. Guinea, Avouris, and F. Xia, "Damping pathways of mid-infrared plasmons in graphene nanostructures," *Nat. Photon.* **7**, 394–399 (2013).

38. B. Sensale-Rodriguez, R. Yan, M. M. Kelly, T. Fang, K. Tahy, W. S. Hwang, D. Jena, L. Liu, and H. G. Xing, "Broadband graphene terahertz modulators enabled by intraband transitions," *Nat. Commun.* **3**, 780 (2012).
39. S. A. Mikhailov, "Graphene-based voltage-tunable coherent terahertz emitter," *Phys. Rev. B* **87**, 115405 (2013).
40. H. Wang, A. Hsu, and T. Palacios, "Graphene electronics for rf applications," *IEEE Microw. Mag.* **13**(4), 114–125 (2012).
41. Tassin, T. Koschny, M. Kafesaki, and C. M. Soukoulis, "A comparison of graphene, superconductors and metals as conductors for metamaterials and plasmonics," *Nat. Photon.* **6**, 259–264 (2012).
42. S. H. Abedinpour, G. Vignale, A. Principi, M. Polini, W.-K. Tse, and A. H. MacDonald, "Drude weight, plasmon dispersion, and ac conductivity in doped graphene sheets," *Phys. Rev. B* **84**, 045429 (2011).
43. C. Hwang, D. A. Siegel, S.-K. Mo, W. Regan, A. Ismach, Y. Zhang, A. Zettl, and A. Lanzara, "Fermi velocity engineering in graphene by substrate modification," *Sci. Rep.* **2** (2012).
44. D. C. Elias, R. V. Gorbachev, A. S. Mayorov, S. V. Morozov, A. A. Zhukov, Blake, L. A. Ponomarenko, I. V. Grigorieva, K. S. Novoselov, F. Guinea, and A. K. Geim, "Dirac cones reshaped by interaction effects in suspended graphene," *Nat. Phys.* **8**, 172–172 (2012).
45. N. Sule and I. Knezevic, "Phonon-limited electron mobility in graphene calculated using tight-binding Bloch waves," *J. Appl. Phys.* **112**, 053702 (2012).
46. A. Konar, T. Fang, and D. Jena, "Effect of high-$\kappa$ gate dielectrics on charge transport in graphene-based field effect transistors," *Phys. Rev. B* **82**, 115452 (2010).
47. I.-T. Lin and J.-M. Liu, "Surface polar optical phonon scattering of carriers in graphene on various substrates," *Appl. Phys. Lett.* **103**, 081606 (2013).
48. N. Rouhi, S. Capdevila, D. Jain, K. Zand, Y. Wang, E. Brown, L. Jofre, and Burke, "Terahertz graphene optics," *Nano Res.* **5**, 667–678 (2012).
49. L. Ju, B. Geng, J. Horng, C. Girit, M. Martin, Z. Hao, H. A. Bechtel, X. Liang, A. Zettl, Y. R. Shen, and F. Wang, "Graphene plasmonics for tunable terahertz metamaterials," *Nature Nanotechnol.* **6**, 630–634 (2011).
50. L. Ren, Q. Zhang, J. Yao, Z. Sun, R. Kaneko, Z. Yan, S. Nanot, Z. Jin, I. Kawayama, M. Tonouchi, J. M. Tour, and J. Kono, "Terahertz and infrared spectroscopy of gated large-area graphene," *Nano Lett.* **12**, 3711–3715 (2012).
51. Y.-W. Tan, Y. Zhang, K. Bolotin, Y. Zhao, S. Adam, E. Hwang, S. Das Sarma, H. Stormer, and Kim, "Measurement of scattering rate and minimum conductivity in graphene," *Phys. Rev. Lett.* **99**(24), 246803 (2007).
52. A. K. Geim and I. V. Grigorieva, "Van der Waals heterostructures," *Nature* **499**, 419-425 (2013).